Master of Science

Preparation of Si/C/rGO granular composites via spray drying method and application as lithium-ion battery anode material

The Graduate School

of the University of Ulsan

Department of Chemical Engineering

Min Jae Kim

Preparation of Si/C/rGO granular composites via spray drying method and application as lithium-ion battery anode material

Supervisor : Professor Won Mook Choi

A Dissertation

Submitted to

the Graduate School of the University of Ulsan

In partial Fulfillment of the Requirements

for the Degree of

Master

by

Min Jae Kim

Department of Chemical Engineering

University of Ulsan, Korea

February 2024

Preparation of Si/C/rGO granular composites via spray drying method and application as lithium-ion battery anode material

This certifies that the master's thesis

of Min Jae Kim is approved.

Committee Chair Prof. Eun Suok Oh

Committee Member Prof. Won Mook Choi

Committee Member Dr. Jeong Hwan Koh

Department of Chemical Engineering

University of Ulsan, Korea

February 2024

Abstract in Korean

리튬이온전지는 최근 몇 년 동안 휴대용 전자 기기, 전기 자동차, 그리고 대규모 에너지 저장 시스템과 같은 다양한 응용 분야에서 널리 사용되고 있습니다. 그러나 에너지 시장의 수요 증가로 인해 에너지 밀도가 높은 차세대 리튬이온 배터리를 개발에 대한 필요성이 증가하고 있습니다. 대안으로 떠오르는 다양한 음극 소재 중 최근 실리콘(Si)이 주목을 받고 있습니다. 실리콘의 이론용량은 4200 mAh g^{-1} 로, 현재 널리 사용되는 흑연의 약 10 배 이상의 높은 이론용량을 가지고 있습니다. 그러나, 실리콘은 충전과정 중에 약 3 배의 급격한 부피 팽창이 발생하여 전극에 손상을 일으키거나 활물질이 집전체에서 탈리되어 리튬이온전지의 내구성 및 전기화학적 성능이 저하되는 문제가 있습니다. 이러한 문제를 해결하기 위해 부피팽창을 억제하는 Si/C 복합체를 개발하거나 Si 표면에 여러 탄소나노재료를 코팅 하는 등 다양한 연구가 진행되고 있습니다. 본 연구에서는 상기한 단점을 해결하기 위해 볼밀과 스프레이 드라이 기법를 이용하여 물리적, 구조적으로 안정된 Si/C/rGO 구형 구조 복합체를 합성하였습니다. 합성된 복합체를 리튬이온전지 음극재로 활용하여 전기화학적 물성들을 테스트한 결과 우수한 전기화학적 특성과 함께 안정한 충/방전 테스트 결과를 보여주었습니다.

Abstract in English

Lithium-ion batteries have been widely utilized in various applications such as portable electronic devices, electric vehicles, and large-scale energy storage systems in recent years. However, the increasing demand in the energy market has led to a growing necessity for the development of next-generation lithium-ion batteries with higher energy densities. Among various alternative anode materials, silicon (Si) has recently gained attention. Silicon boasts a theoretical capacity of 4200 mAh g^{-1}, which is more than ten times higher than the widely used graphite. However, silicon experiences a significant threefold expansion in volume during the charging process, leading to electrode damage or the detachment of active material, resulting in reduced durability and electrochemical performance of lithium-ion batteries. To address these issues, various studies are underway, including the development of Si/C composites to suppress volume expansion or coating silicon surfaces with various carbon nanomaterials. In this study, to address the aforementioned drawbacks, a physically and structurally stable Si/C/rGO granular structure composite was manufactured using ball milling and spray drying techniques. Testing this composite as the anode material in lithium-ion batteries demonstrated excellent electrochemical characteristics and remarkable stability according to charge/discharge cycle test.

Keywords: *Lithium ion battery, Silicon, Anode materials, Spray drying*

Table of contents

List of figures

Figure 30. FE-TEM and EDS mapping images of Si-20 after 100 cycle test with elements as Si, C, and O

CHAPTER 1. Introduction

1.1. Lithium-ion Batteries

Fossil fuel-based vehicles contribute to environmental issues through air pollution and greenhouse gas emissions, necessitating a response to address these challenges. As an alternative solution to these environmental problems, electric vehicles have emerged. Electric cars, by not relying on fossil fuels, can reduce air pollution and greenhouse gas emissions, gaining recognition as an eco-friendly mode of transportation. [1,2]

In addition, the lithium-ion battery, a core component of electric vehicles, possesses various advantages. Firstly, it boasts excellent energy density, enabling electric cars to exhibit high performance and cover longer distances, coupled with a high cycle stability that extends its lifespan. The rapid charging and discharging capabilities enhance the efficiency of electric vehicles, while the use of environmentally friendly materials helps reduce the overall environmental impact. Moreover, the relative affordability of lithium and advancements in recycling technologies contribute to improving the economic viability of electric vehicles [3].

The combined effects of these features highlight the role of electric vehicles and lithium-ion batteries in promoting sustainable mobility and environmental conservation. By reducing dependence on fossil fuels and offering an environmentally friendly alternative, electric vehicles and lithium-ion batteries play a crucial role in addressing air pollution and climate change in contemporary society.

In recent years, lithium-ion batteries (LIBs) have become predominant in various power applications, such as portable electronic devices, electric vehicles (EVs), and large-scale storage systems, owing to their notable features like high capacity, extended lifespan, and environmental friendliness. However, due to the escalating energy market demands, there is an urgent need to create the next generation of LIBs with increased energy and power densities. Traditional anode materials like graphite are insufficient in meeting the demands for significantly higher energy/power densities and prolonged cycle life due to their limited theoretical capacity (372 mAh g^{-1}) and low energy density (~150 Wh kg^{-1}) [4].

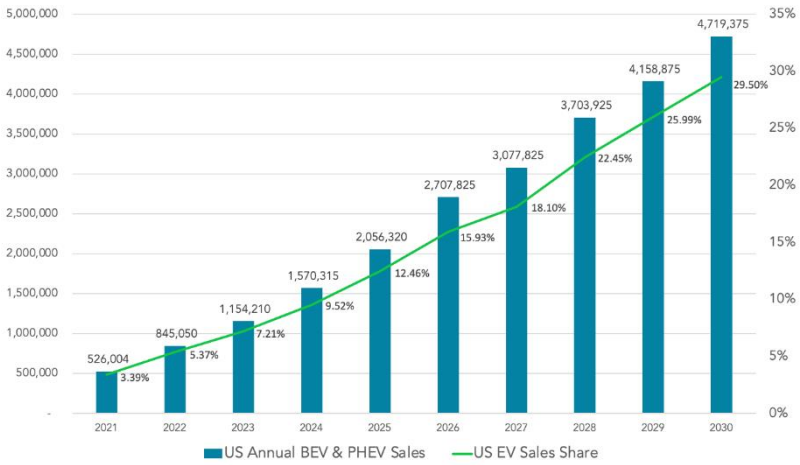

Figure 1. US Electric vehicle sales forecast, 2021-2030 (Source : EVAdoption)

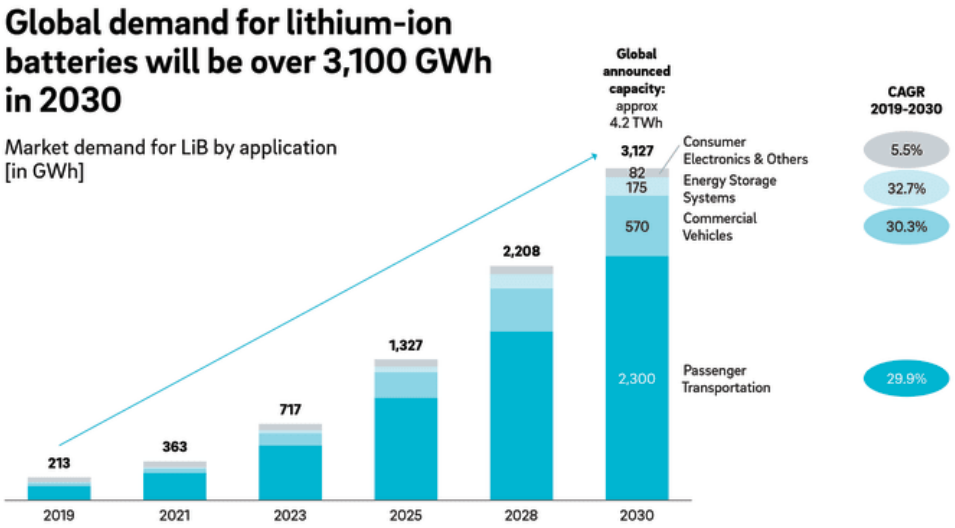

Figure 2. Forecast of increasing demand for lithium-ion battery capacity
(Source : Avicenne, Fraunhofer, HIS Markit, Roland Berger)

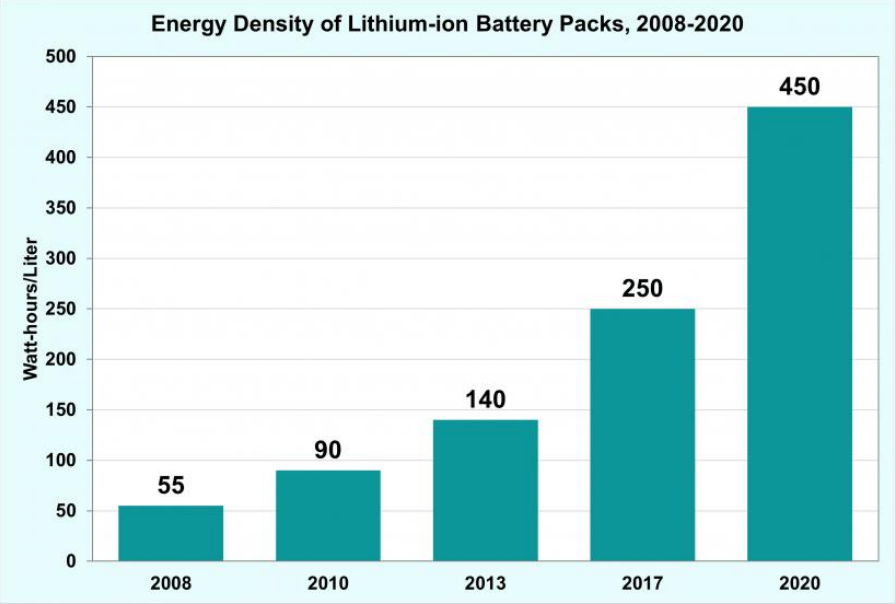

Figure 3. Trend in energy density of lithium-ion battery, 2008-2020, [5]

1.2. Anode materials of Lithium-ion Matteries

Over an extended period, researchers have been dedicated to developing advanced anode materials characterized by high abundance, low cost, and excellent lithium-ion storage properties. Various anode materials for LIBs have been explored, including Li4Ti5O12, transition metal oxides (MnO, Nb2O5, NiO, etc.), transition metal sulfides (Ni2S3, MoS2, VS2, etc.), and alloys (Sb, Sn). Among these, silicon (Si) has recently gained increasing attention as one of the most promising alternatives to graphite.

The maximum theoretical capacity of silicon is 4200 mAh g^{-1}, which is 10 times that of graphite. This is attributed to the ability of a single silicon atom to bond with approximately four lithium ions ($Li_{4.4}Si$). Additionally, silicon exhibits a lithiation potential for Li/Li+ of 0.4 V, higher than that of graphite (approximately 0.05 V), which inhibits the formation of lithium plating and dendrites [6].

A significant aspect is that silicon holds the second-largest storage capacity on Earth, exceeding 28% of the Earth's total mass. It is widely available in nature in various forms such as mineral silicates, solar panels, rice husks, straw, bamboo stalks, and sugarcane. Most of these mentioned resources are challenging to recycle with high added value or low environmental pollution. Therefore, developing strategies to harness silicon resources in energy storage systems holds substantial value for advanced electrodes in next-generation lithium-ion batteries and environmentally friendly sustainable development.

Regrettably, significant challenges continue to impede the commercial viability of silicon (Si). Si undergoes substantial volume expansion during lithiation, a phenomenon verified through imaging techniques and the documentation of various Li–Si phases. This volumetric expansion imposes increased stress on the Si, leading to the generation of Si powder. Furthermore, the expansion prompts the displacement of conductive material from the surface of the active material, resulting in diminished electrochemical performance [7,8].

In the initial lithiation process, a solid electrolyte interphase (SEI) forms on the surface of the silicon electrode through the electrolyte's decomposition. While SEI facilitates lithium-ion conduction, it impedes electron flow, thereby constraining electrolyte consumption and enhancing the cycling performance of the lithium-ion battery. The electrochemical efficacy of lithium-ion batteries is notably contingent on the quality of the SEI. However, due to Si's volume expansion, the organic components in the electrolyte decompose, leading to the formation of an unstable SEI. This precarious SEI is prone to rupture and reform on the Si surface, perpetually consuming significant amounts of lithium ions, diminishing the initial Coulombic efficiency (ICE), and ultimately depleting the electrolyte. Beyond the challenges arising during cycling, Si poses additional hurdles as a semiconductor material with poor conductivity in a metastable structure [9,10].

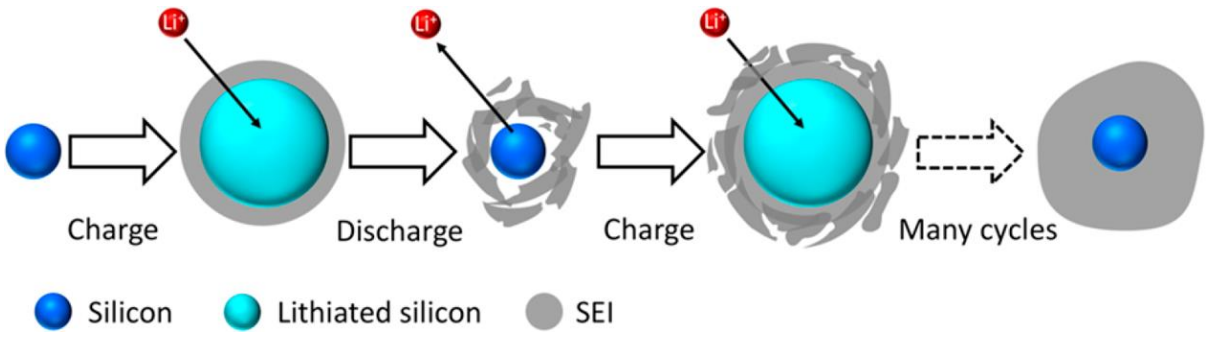

Figure 4. Schematic of SEI formation occurring at the surface of silicon upon electrochemical cycling, [11]

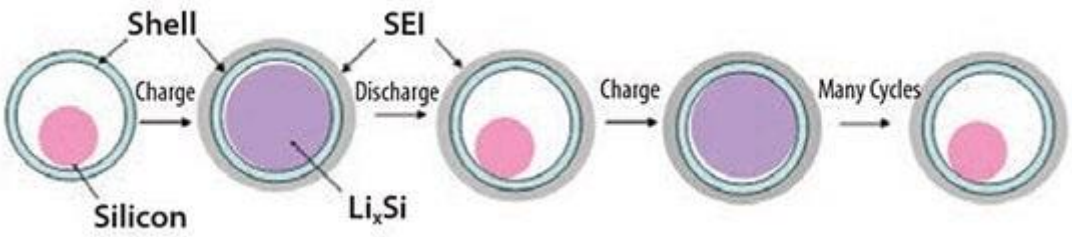

Figure 5. Schematic of yolk–shell structured Si hybrid, [12]

1.3. Research Strategy

To overcome the well-known drawbacks of silicon-based anode materials, extensive research has been conducted, focusing on special structural designs such as core-shell, porous, and yolk-shell structures. Additionally, silicon-based composite materials have been fabricated, contributing to a significant enhancement of electrochemical performance.

One of the most promising strategies for practical application involves synthesizing silicon/carbon composite anode materials with a well-designed structure [13]. Introducing a carbon phase is believed to improve the electronic conductivity of the composite and accommodate the substantial volume changes of silicon during lithium insertion/extraction processes. Given graphene's superior electrical conductivity, various hybrid nanomaterials combining graphene with active materials have been fabricated and utilized as electrodes for lithium-ion batteries (LIBs) [14]. Furthermore, numerous well-designed Si/graphene nanocomposites have demonstrated enhanced electrochemical performance. However, many of these composites exhibit low initial Coulombic efficiency due to the large specific surface area of graphene and the direct contact between Si and the electrolyte [15]. And the practical application of nano-sized silicon-based composite materials has been delayed due to low tap density and inadequate scalability. Therefore, there is a need for silicon-based composites with fine design and scalable synthetic processes, equipped with expressive carbon anode materials as an alternative. ball milling represents another critical procedure in shaping nanostructures and refining materials into smaller particle sizes. Ball milling serves as a valuable technique, inducing collisions and friction in materials to reduce particle size, amplify surface area, and improve electrochemical performance. This technology is actively explored in the realms of nanotechnology and energy storage materials [16]. Moreover, the spray drying technique, known for its high production efficiency, has been widely employed in the industrial production of catalysts and pharmaceutical carriers. Significant efforts have been directed towards the synthesis of Si-based composites through the spray drying process [17].

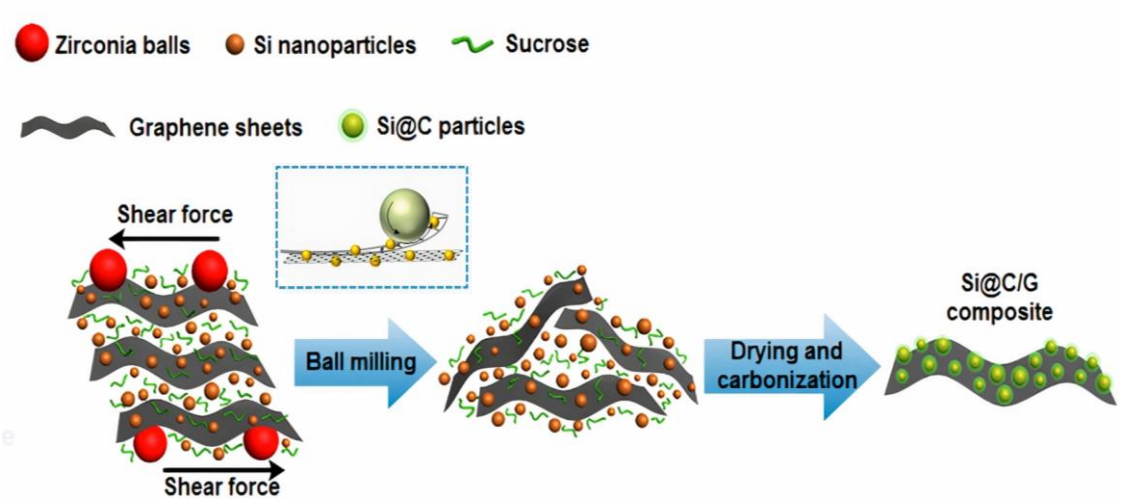

Figure 6. Scheme of ball milling mechanism in Si/C/GO composite

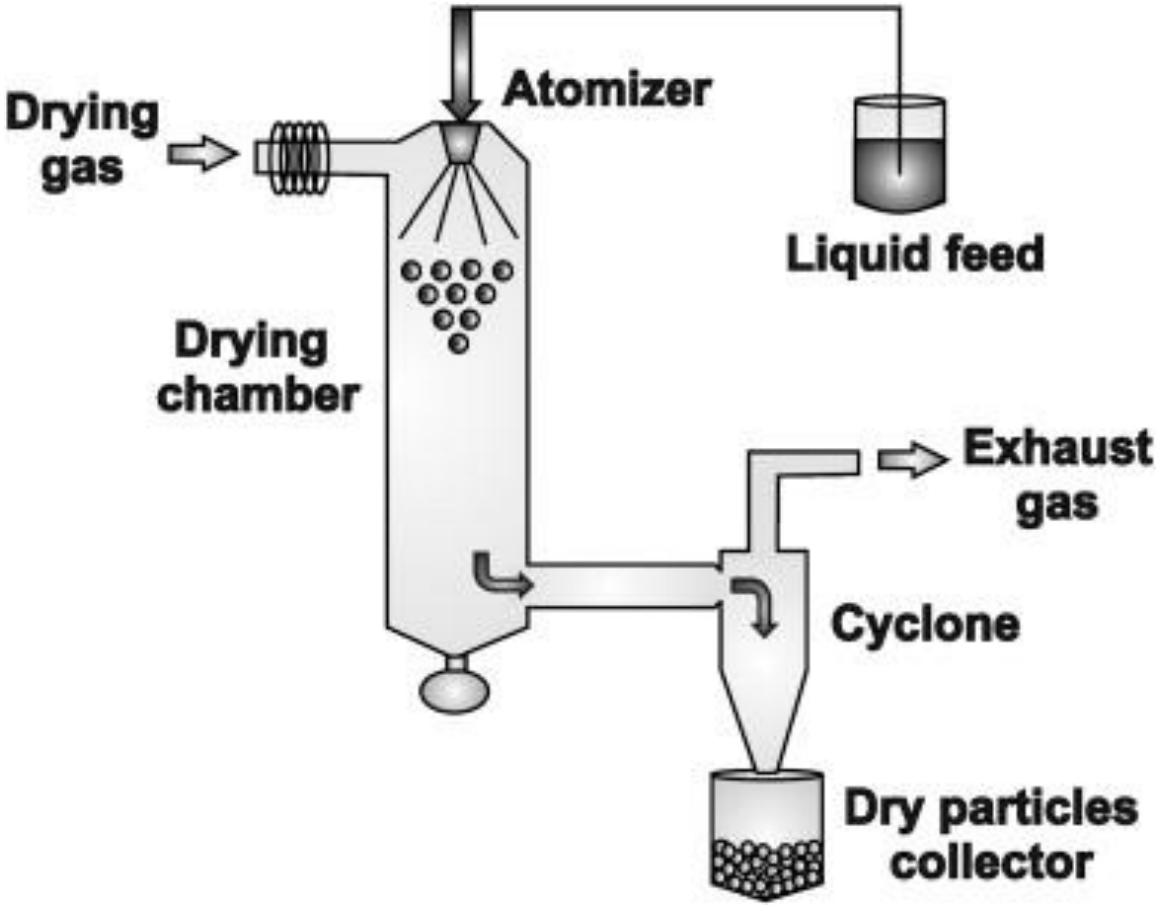

Figure 7. Scheme of spray-drying mechanism / [sp]

CHAPTER 2. Experimental

2.1. Preparation of Si/C/rGO Composite

100mg of silicon (~100 nm Si powder), 363mg of graphene oxide, 37mg of dextrose, and 200ml of DI water were mixed using a high-energy ball mill at 300rpm, 1 hour. Following this, the solution was stirred with a magnetic bar at 300rpm while being fed into a spray dryer with an inlet temperature of 180 degrees. The dried samples were then subjected to thermal reduction at 800 degrees for 2 hours in a nitrogen condition using a vacuum oven to yield Si/C/rGO composite. As a comparison, the preparation of the physical mixing composite and ball milled composite is similar to that of the Si/C/rGO composite but without the process of ball milling and spray drying. Also, To determine the optimal weight percentage of silicon in the composite, silicon samples were synthesized at 10% intervals from 10% to 40%.

2.2. Electrode Fabrication

The slurry consisted of a uniform blend of anode material powder, carbon black, styrene-butadiene rubber(SBR) binder and carboxymethyl cellulose(CMC) 1wt% solution binder that was dissolved in DI water. The weight ratio of active material, conductive additive, and binder was 60:20:20. The electrodes were fabricated by slurry casting on copper foil with a coater, which was then dried for 12hr at 70°C. After drying, a roll press was used to compress the electrode and current collector together.

2.3. Half Coin Cell Assembly

An argon-filled glovebox was used to fabricate CR-2032 size coin cells. The coin cell was composed of lithium metal as the counter electrode, a polyethylene membrane as the separator, and an organic electrolyte. The electrolyte was a mixture of lithium hexafluorophosphate (1.15M LiPF6) dissolved in a mixture of solvent ethylene carbonate (EC), fluoroethylene carbonate (FEC), propylene carbonate (PC), diethyl carbonate (DEC), and ethyl methyl carbonate (EMC) in a volume ratio of 20:10:5:40:25. Each coin-half cell was allowed to rest for one day before undergoing electrochemical tests.

2.4. Characterization

The Field emission scanning electron microscope (FE-SEM) were acquired on the JSM-7600 (JEOL). The high-resolution transmission electron microscope (HRTEM) images were acquired on JEM-2100F (JEOL). X-ray diffraction patterns (XRD) of the samples were acquired by the ULTIMA 4 (Rigaku) at 10-80° with a scanning rate 0.02°/sec. To verify the functional groups in samples were measured by Raman spectroscopy (RAMAN). Thermogravimetric analysis(TGA) were conducted to confirm the silicon content.

2.5. Electrochemical Performance

A battery performance evaluation system (WonATech Co., Ltd, WBCS3000) was used to test the electrochemical performance including cyclic voltammetry(CV) within a voltage window of 0.005-1.5 V vs. Li/Li^+. The cycling test, conducted to evaluate the lifespan characteristics of the battery, used current densities of 0.1 and 0.5C. The rate capability test, aimed at examining the battery's high-rate performance, utilized current densities ranging from 0.1 to 5C. Using an electrochemical analyzer (BioLogic Science Instrument, VSP), electrochemical impedance spectroscopy (EIS) tests were performed. The EIS test was conducted to investigate the electrochemical resistance of the cells based on their equivalent circuit models.

CHAPTER 3. Results and Discussion

3.1. FE-SEM/EDS Analysis

In the case of PM (Physical Mixing), the SEM analysis revealed that, through the use of sinki, a physical mixing method, the silicon covers the surface of the graphene oxide sheet. However, when stirring is carried out using a ball mill, it was observed that silicon particles are embedded in the graphene oxide sheet, indicating that the graphene sheet encapsulates the silicon, physically inhibiting expansion. For the sample prepared using spray drying, the particle structure was modified into a spherical shape, and this spherical structure contributes to stability during expansion/contraction. Furthermore, through EDS analysis, it was confirmed that in the case of the spray-dried sample, a successful synthesis of a spherical structure composed of silicon and reduced graphene oxide was achieved.

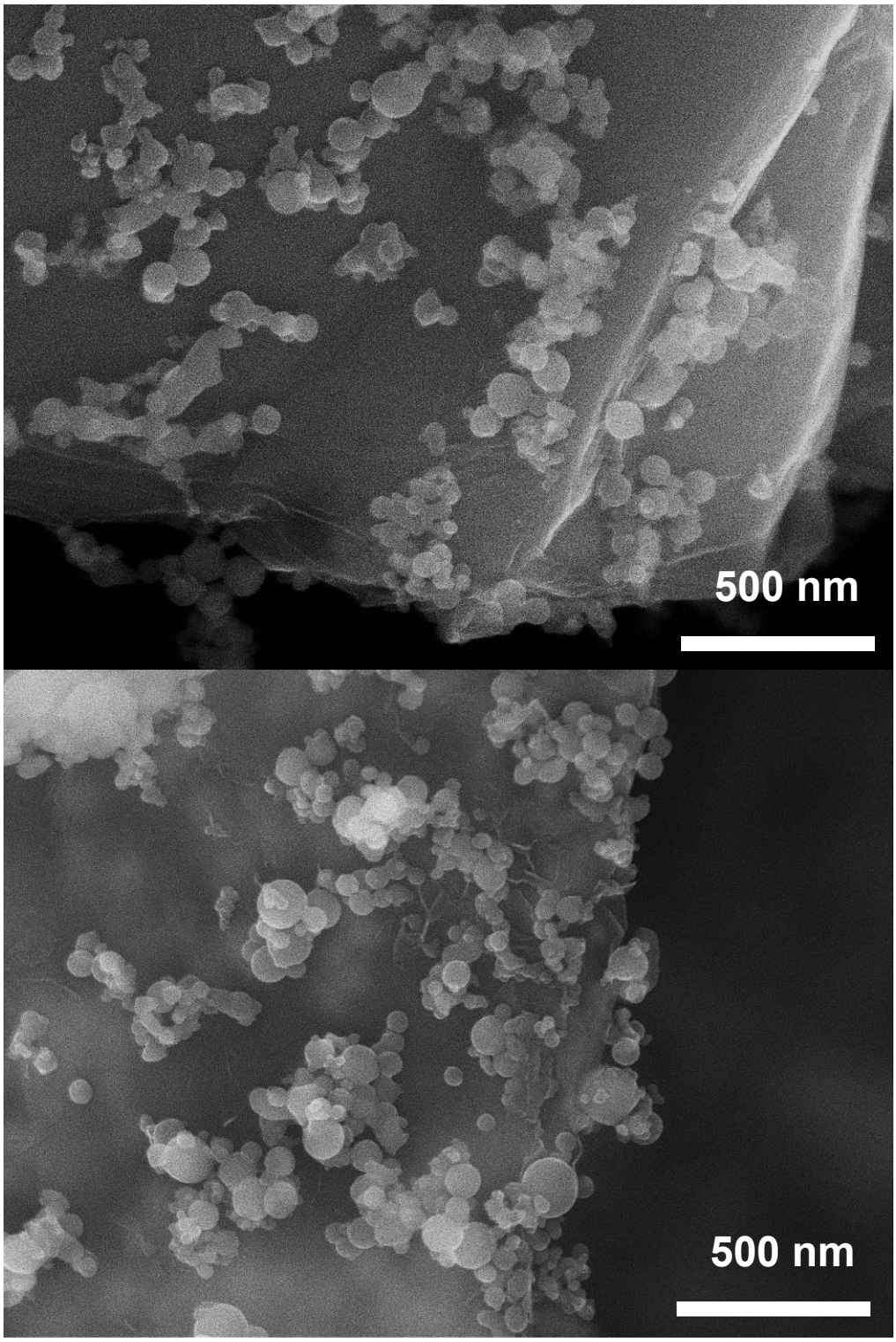

Figure 8. FE-SEM images of Physically mixed(PM)

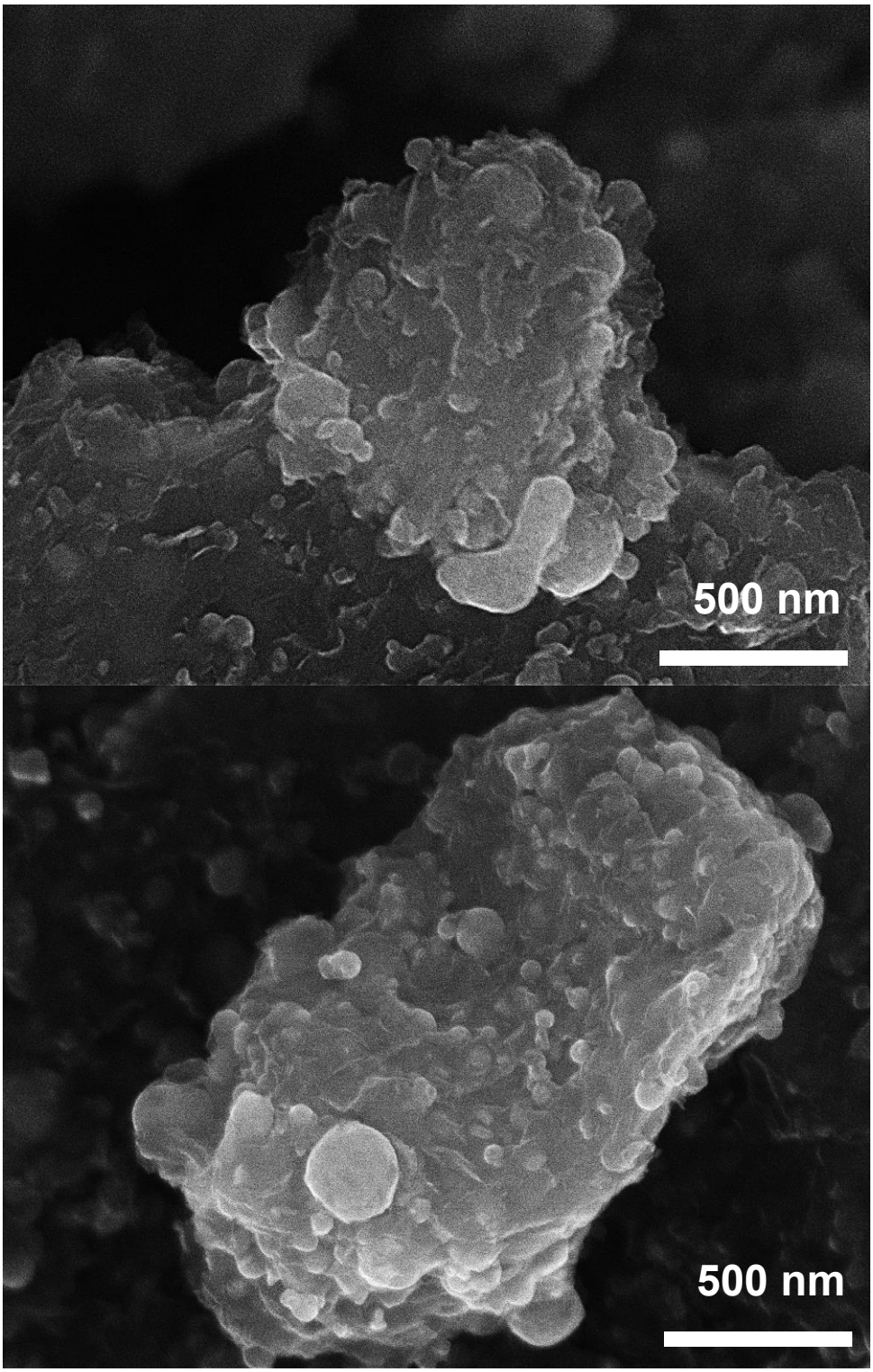

Figure 9. FE-SEM images of Ball milled(BM)

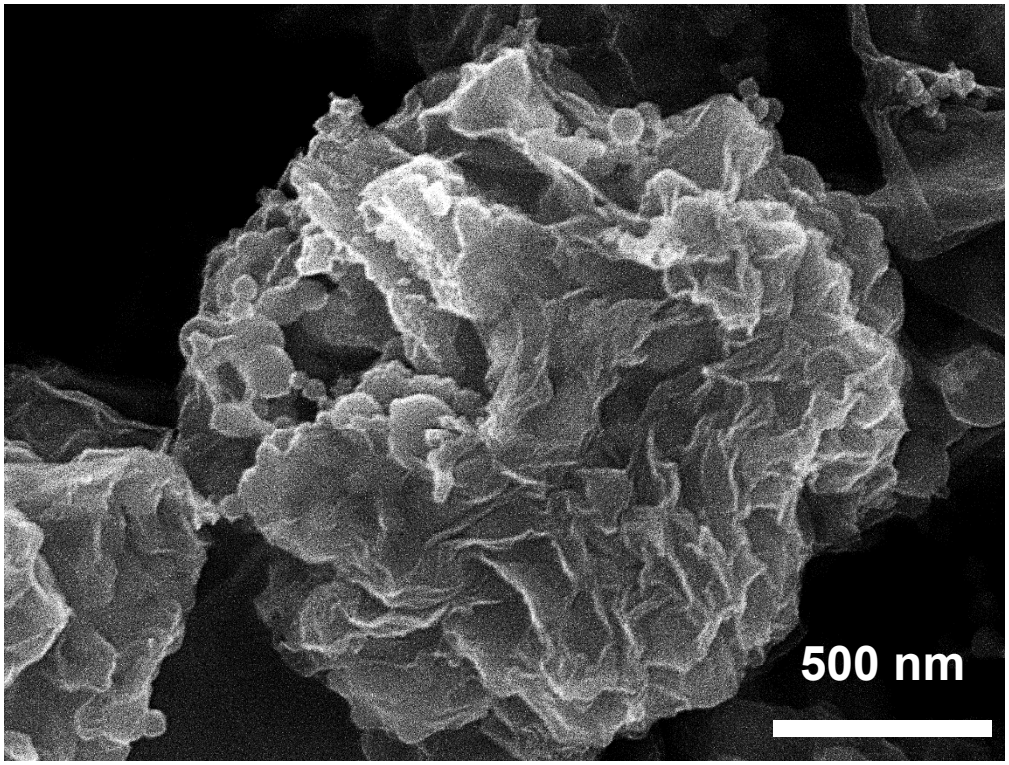

Figure 10. FE-SEM images of Spray dried Si/C/rGO

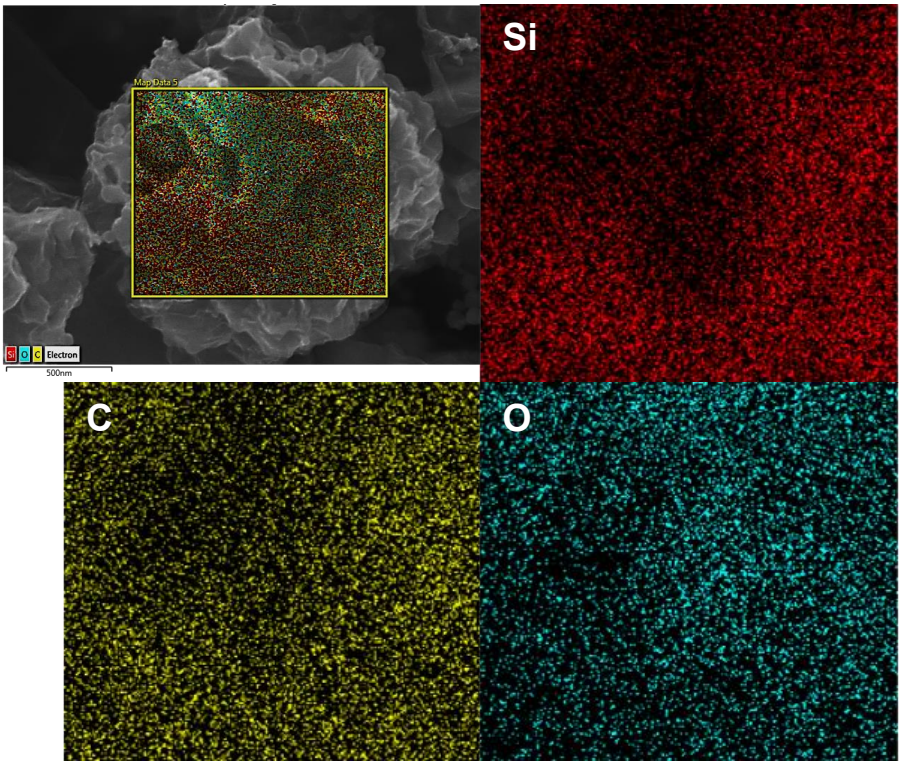

Figure 11. FE-SEM EDS mapping of Spray dried Si/C/rGO with elements as Si, C, and O

3.2. FE-TEM/EDS Analysis

TEM/EDS analysis revealed that in the ball-milled sample, the presence of silicon embedded in graphene oxide sheets was more distinct. This suggests that, unlike conventional physical mixing methods, graphene more efficiently contacts the silicon surface. In the Si/C/rGO sample, it was observed that nano silicon particles were wrapped in thin graphene sheets, and this was further confirmed by EDS. STEM analysis showed the outermost layer of the sample to consist of graphene sheets, followed by carbon layers, and the presence of silicon (111) crystal structure.

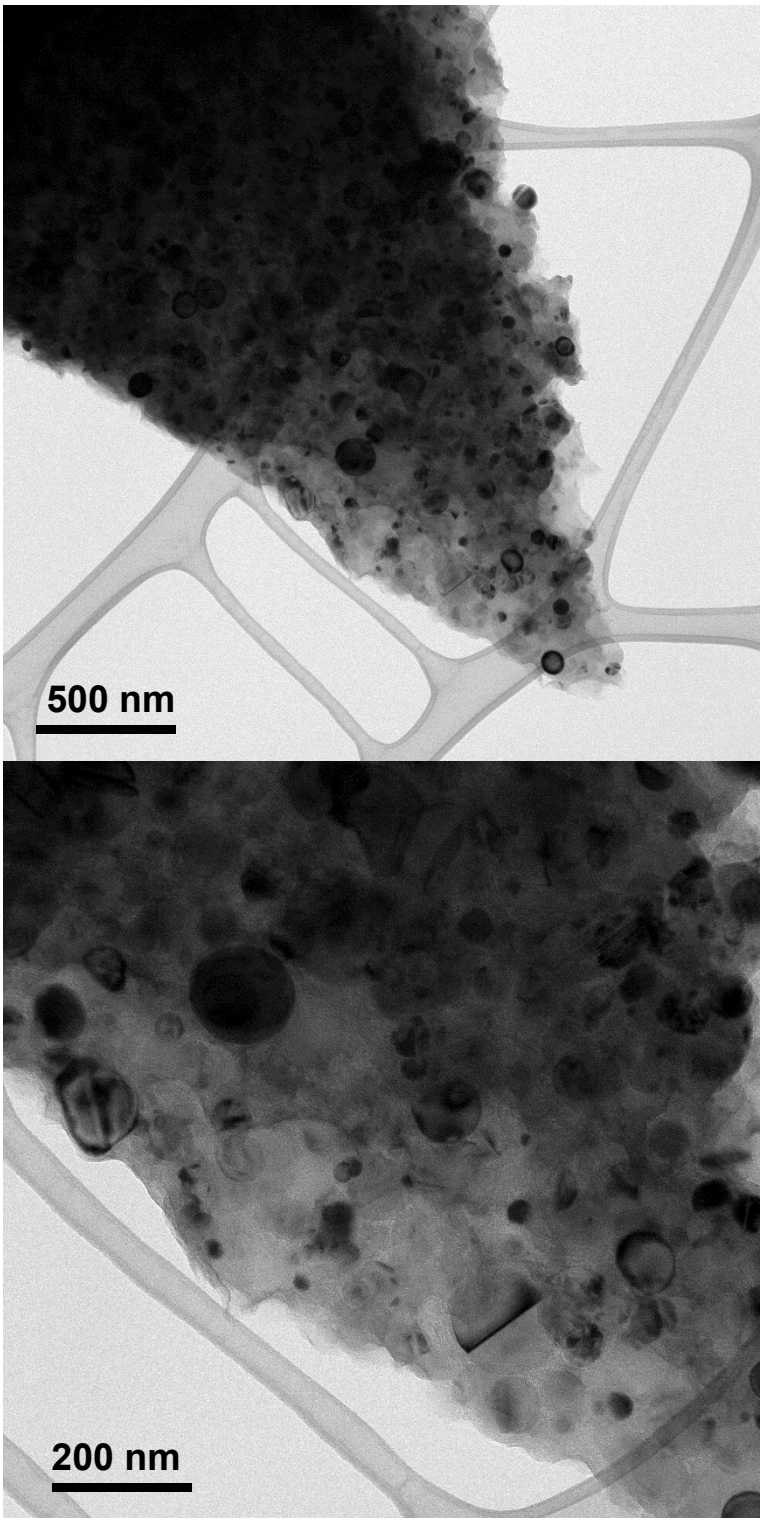

Figure 12. FE-TEM images of BM

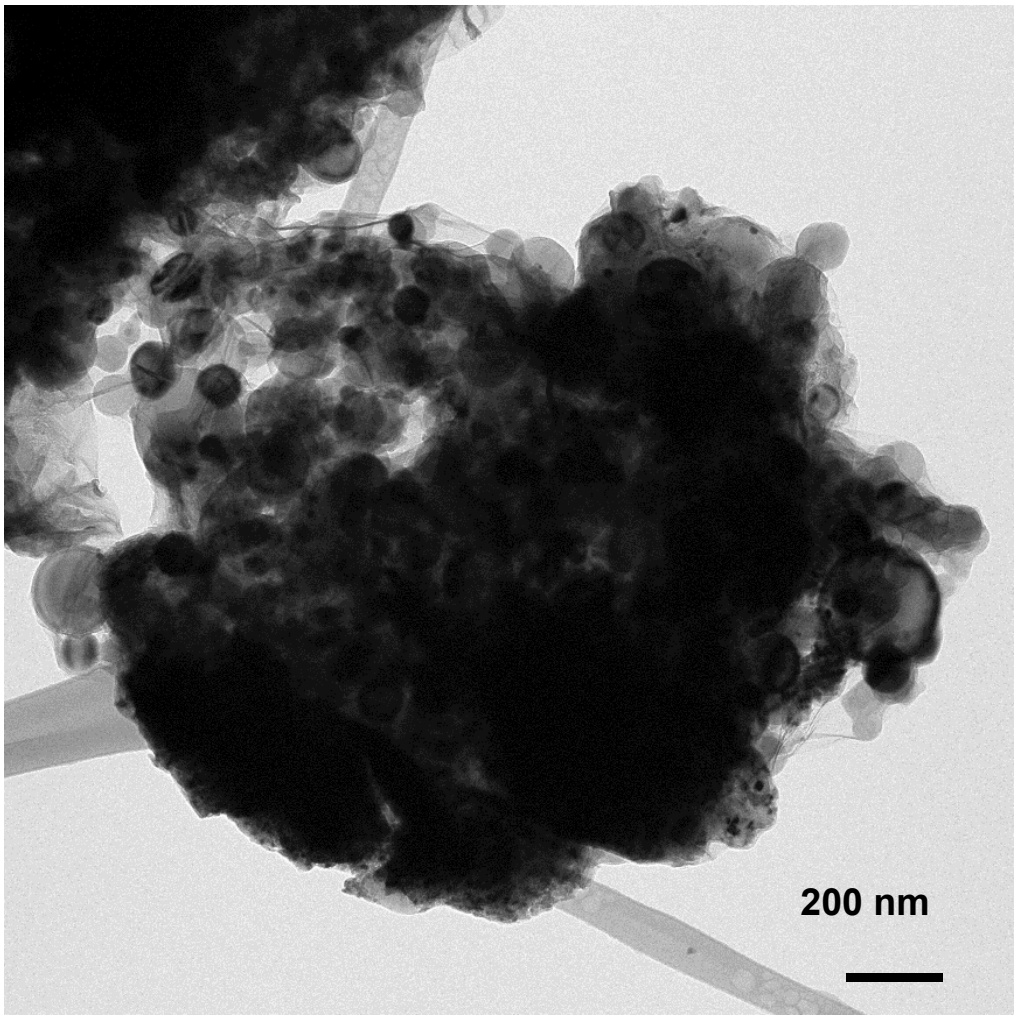

Figure 13. FE-TEM images of Spray dried Si/C/rGO

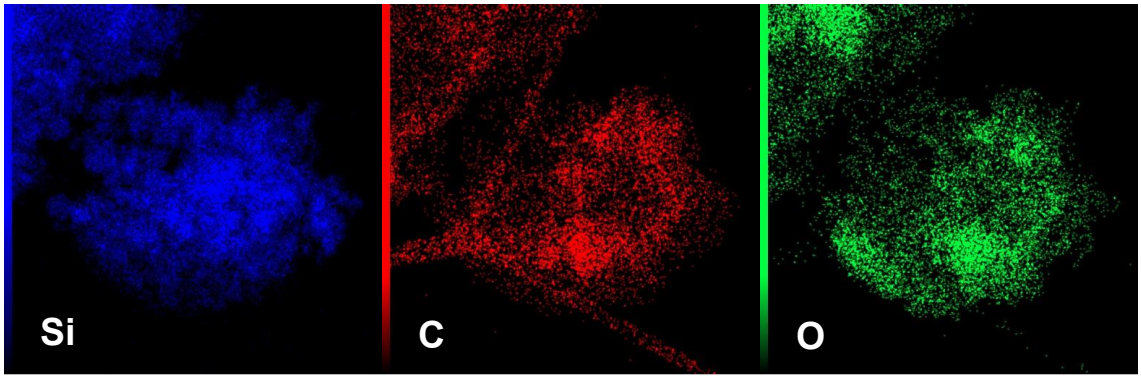

Figure 14. FE-TEM EDS mapping of Spray dried Si/C/rGO with elements as Si, C, and O

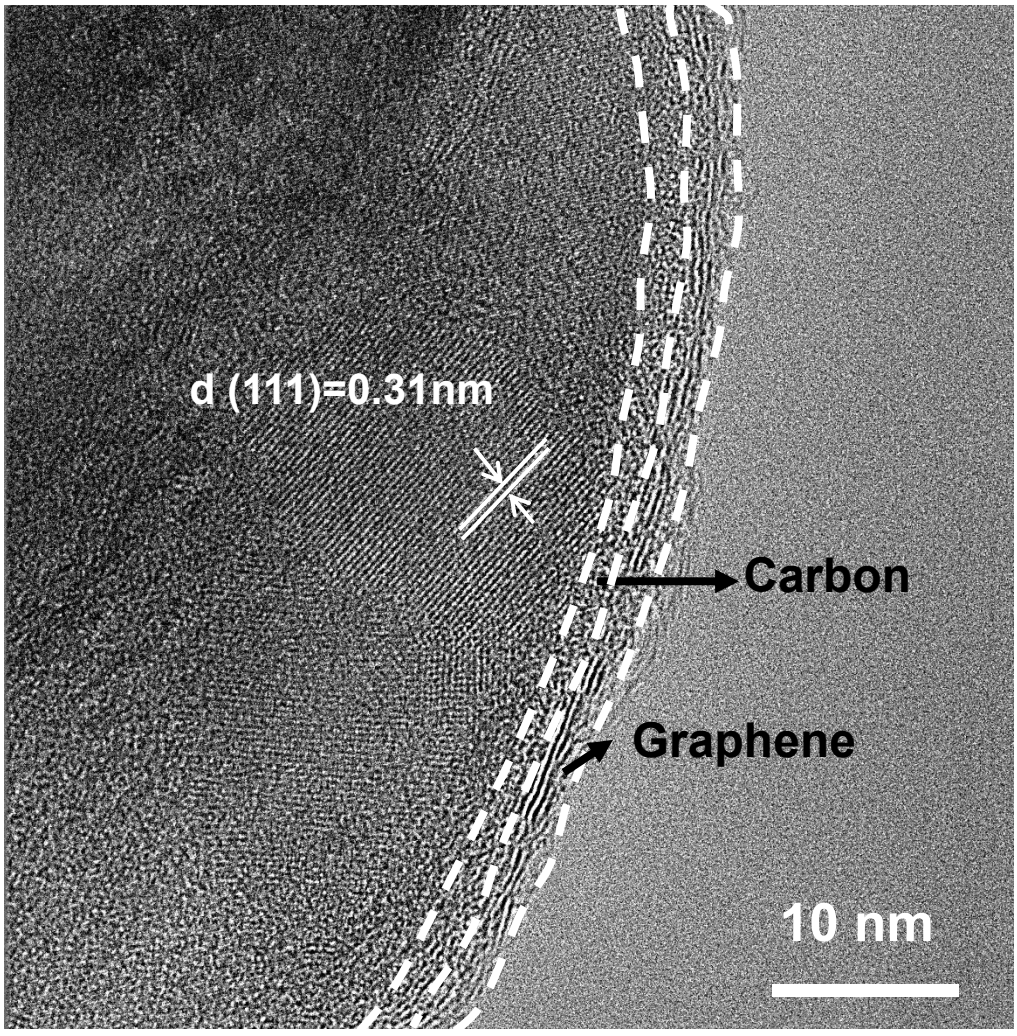

Figure 15. FE-TEM high magnification images of Spray dried Si/C/rGO

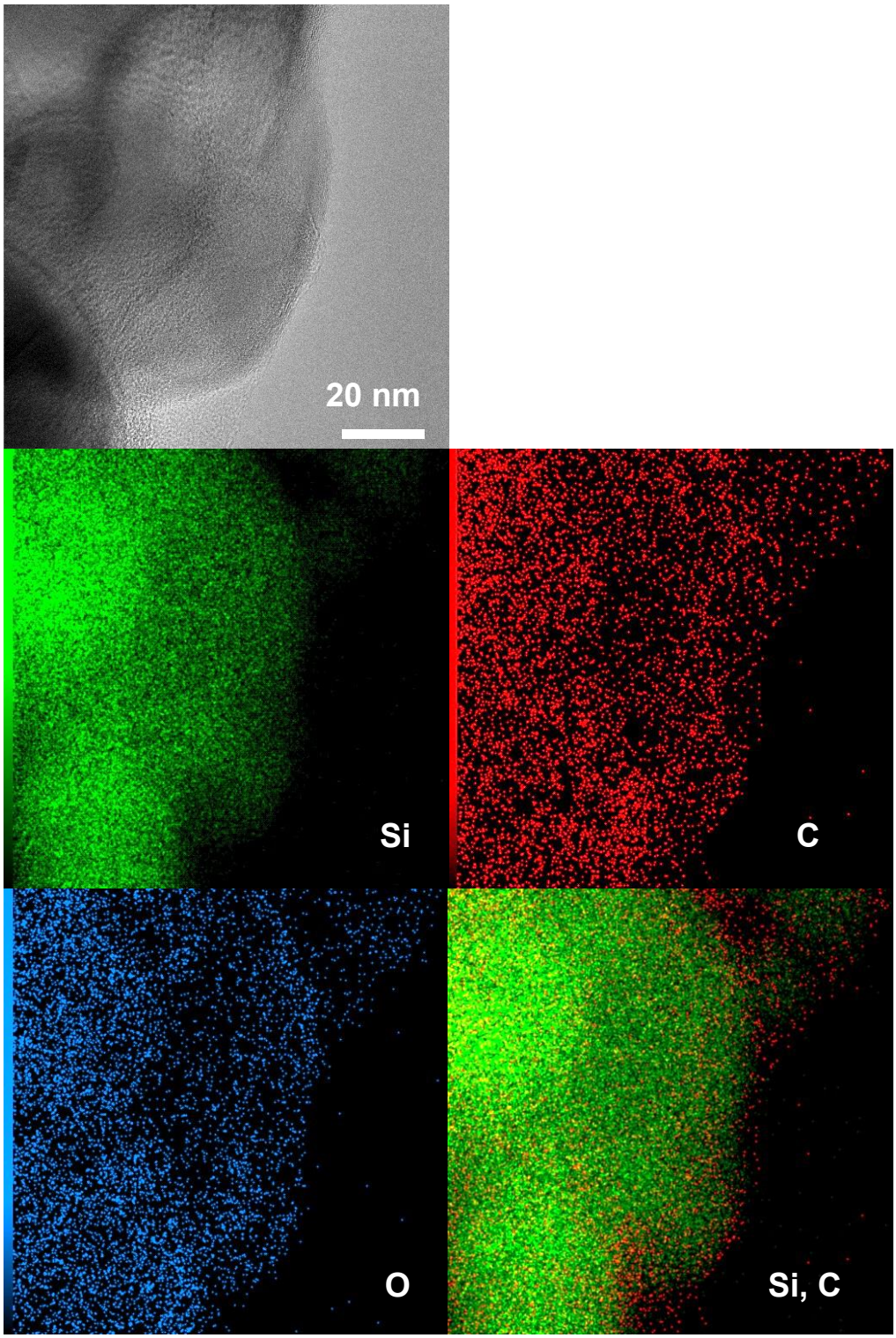

Figure 16. FE-TEM EDS high magnification mapping images of Spray dried Si/C/rGO with elements as Si, C, O, and Si with C

3.3. XRD Analysis

The XRD results display the XRD patterns of Si, rGO, BM, and Si/C/rGO. There is no significant difference between the spectra, and sharp diffraction peaks corresponding to crystalline silicon and the rGO (002) peak appear in the XRD patterns of BM and Si/C/rGO.

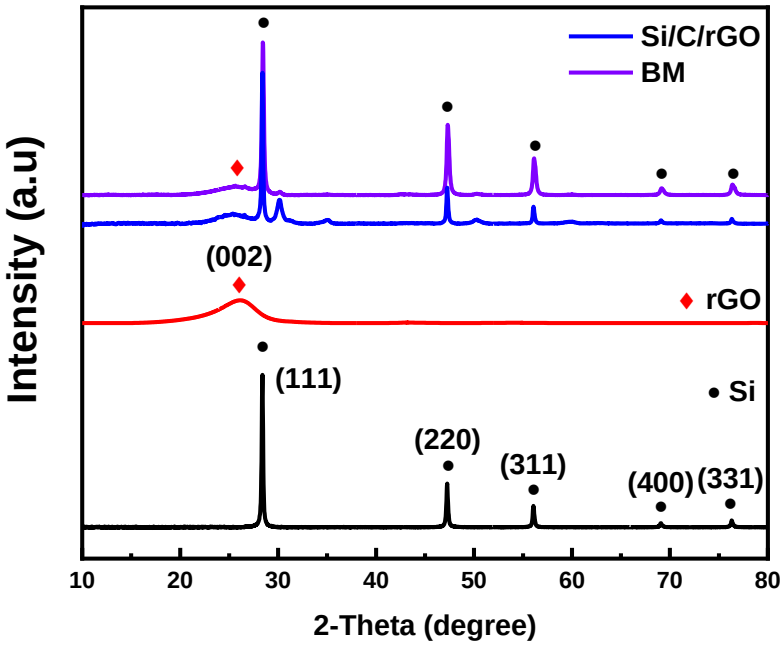

Figure 17. XRD patterns of Si, rGO, PM, BM, and Si/C/rGO

3.4. Raman Analysis

The Raman results show the Raman spectra of Si, BM, and Si/C/rGO. The spectra exhibit sharp peaks at around 510 cm^{-1}, associated with the characteristic signals of crystalline silicon in all three spectra [18]. The Raman spectra of BM and Si/C/rGO show characteristic peaks of graphene at approximately 1350 (D peak) and 1580 (G peak) [19]. This indicates the stable formation of a composite of silicon and rGO.

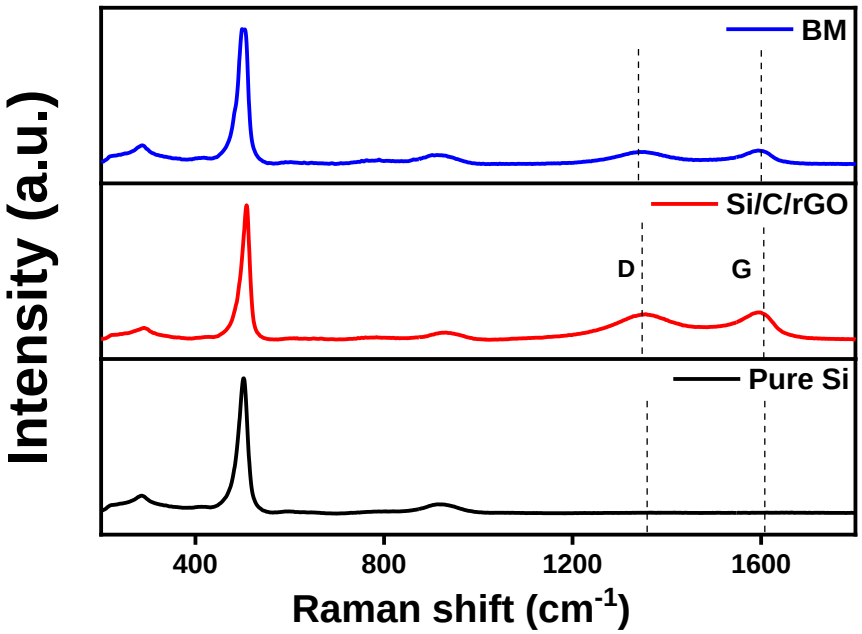

Figure 18. Raman spectra of Pure Si, BM, and Si/C/rGO

3.5. Electrochemical Performance

3.5.1. Cyclic Voltammetry Analysis

The Si/C/rGO anode was measured from 0.005 to 1.5 V at a scan rate of 0.1 mV/s. The peak observed in the first cycle between 0.3 and 0.8 V, disappearing in subsequent cycles, is mainly attributed to the formation of the Solid Electrolyte Interface (SEI) layer's nonflammable nature[20,21]. The strong peak at 0.01 V during the initial discharge process corresponds to the lithiation of crystalline silicon, and subsequent delithiation processes occurred at 0.31 V and 0.51 V. The peaks at 0.17 V during discharge and at 0.33 V and 0.54 V during charge in the following cycles are interpreted as the repetitive lithiation/delithiation processes of amorphous silicon. Peaks corresponding to the lithiation/delithiation processes of carbon and graphene, however, are obscured by intense peaks corresponding to the alloying/dealloying process of silicon[22,23,24].

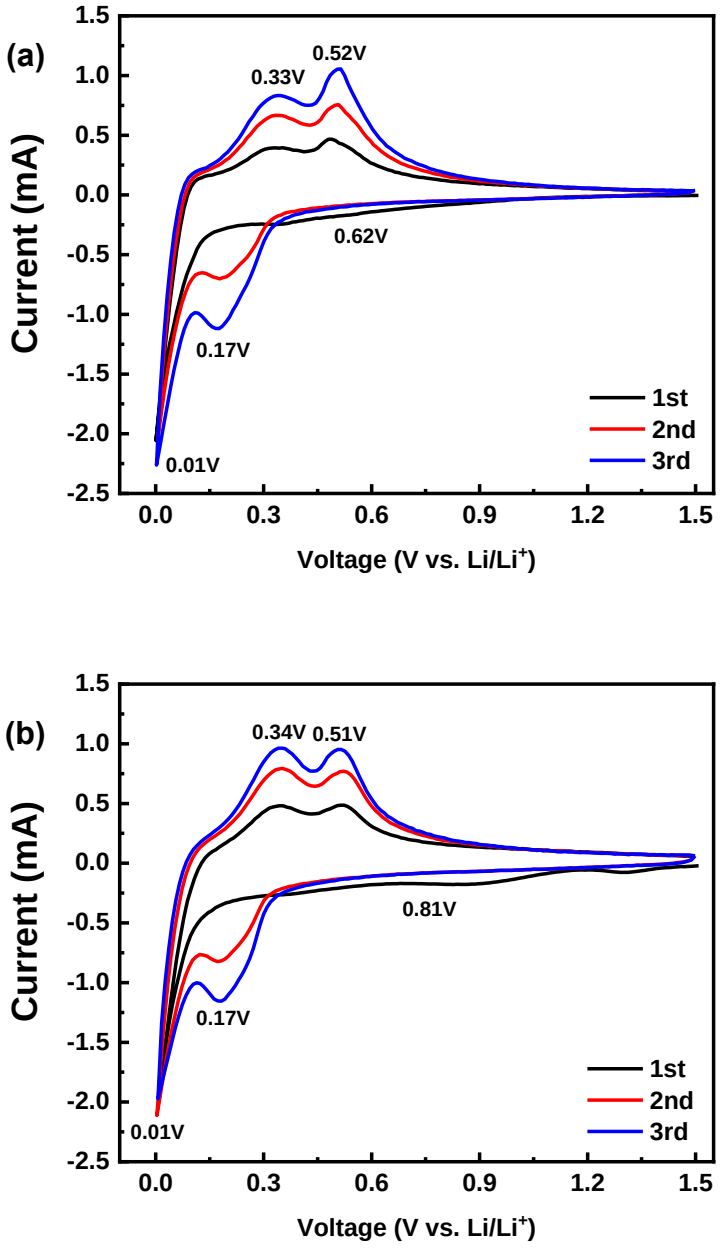

Figure 19. CV curves of (a) BM and (b) Si/C/rGO for the first three cycles

3.5.2. Cycling test

The cycle test results indicate that the PM sample exhibits capacity changes similar to pure silicon due to structural instability. On the other hand, the BM sample shows a tendency for stability up to 100 cycles as silicon particles are embedded in the rGO sheet, suppressing the volume expansion of silicon. However, it exhibits an initial capacity loss, likely attributed to physical damage during the ball milling process, leading to increased resistance.

In contrast, the Si/C/rGO sample demonstrates excellent initial capacity in all samples. However, Si-30 and Si-40 show reduced stability due to excessively high silicon content. Therefore, Si-20, with 20wt% silicon using both ball milling and a spray dryer, shows the best performance. The Si-20 sample exhibits approximately 65% capacity retention after 250 cycles. This trend is consistent in a full cell with NCM 622 at a 1.1 N/P ratio.

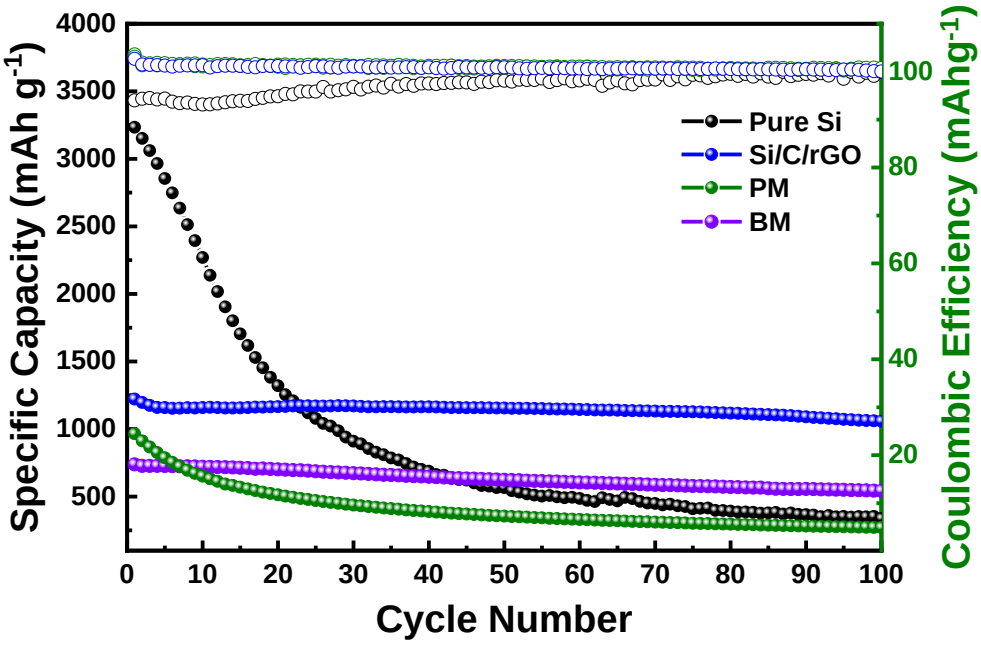

Figure 20. Cycling performances of Pure Si, PM, and BM

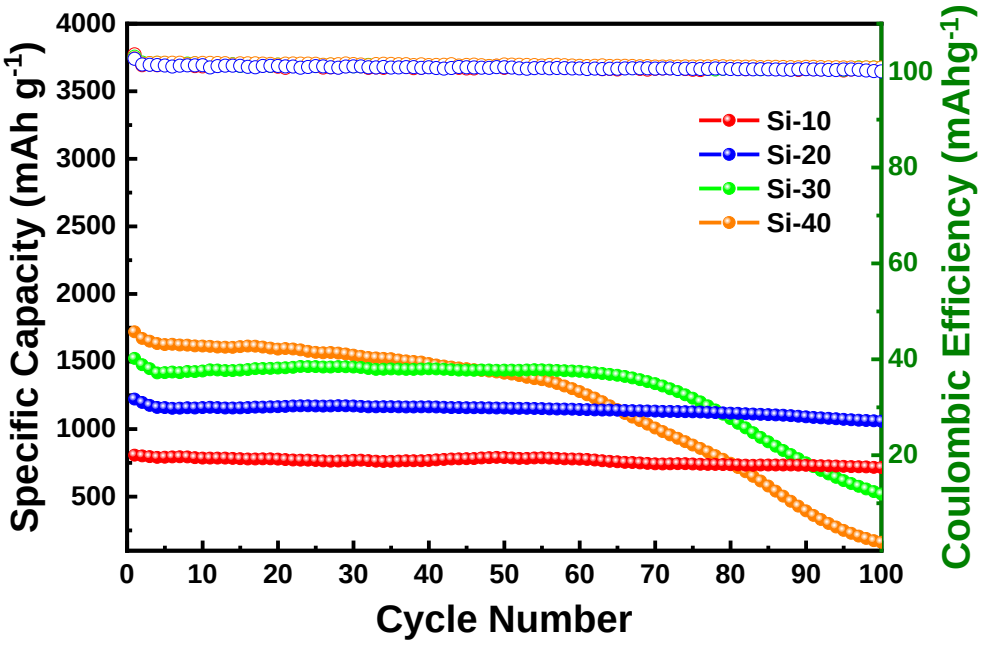

Figure 21. Cycling performances of Si-10, Si-20, Si-40, and Si-40

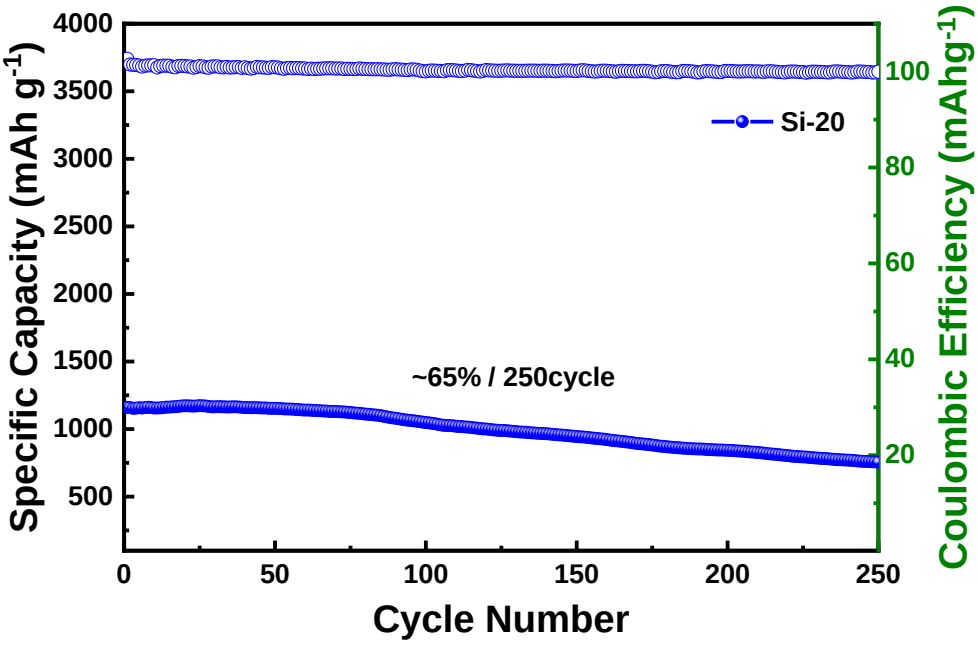

Figure 22. Long-term cycling performance of the Si-20

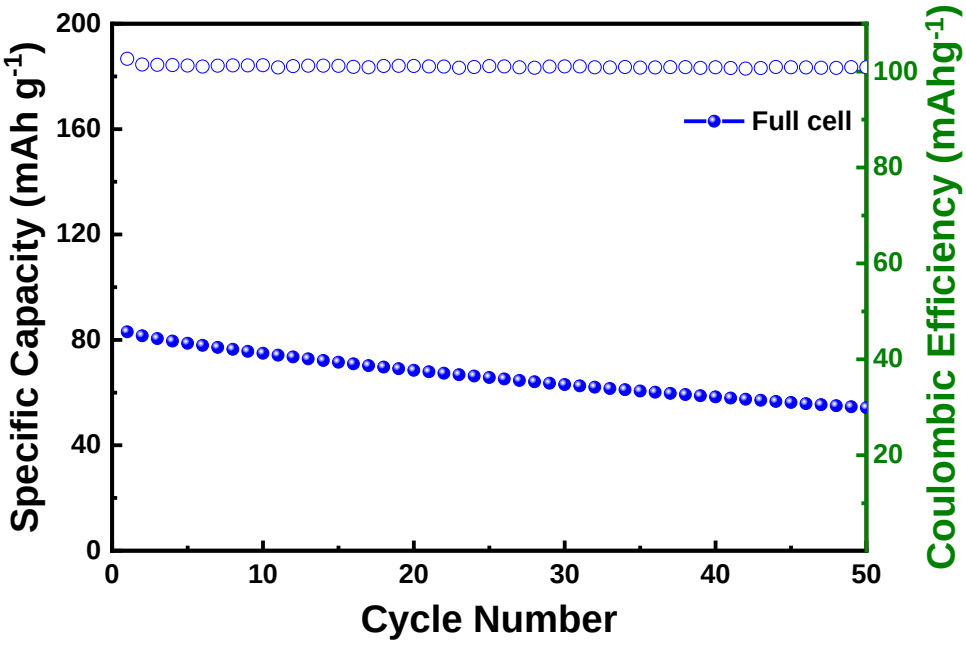

Figure 23. Cycling performance of the full cell with Si-20/NCM 622

3.5.3. Rate Capability

Rate capability results show a similar trend to the cycle test outcomes. In the case of the PM sample, it fails to provide initial 0.1C capacity recovery after charging up to 5C. The BM sample exhibits excellent capacity recovery but shows a lower initial capacity compared to the same silicon content. In contrast, the Si-20 sample demonstrates both outstanding initial capacity and capacity recovery.

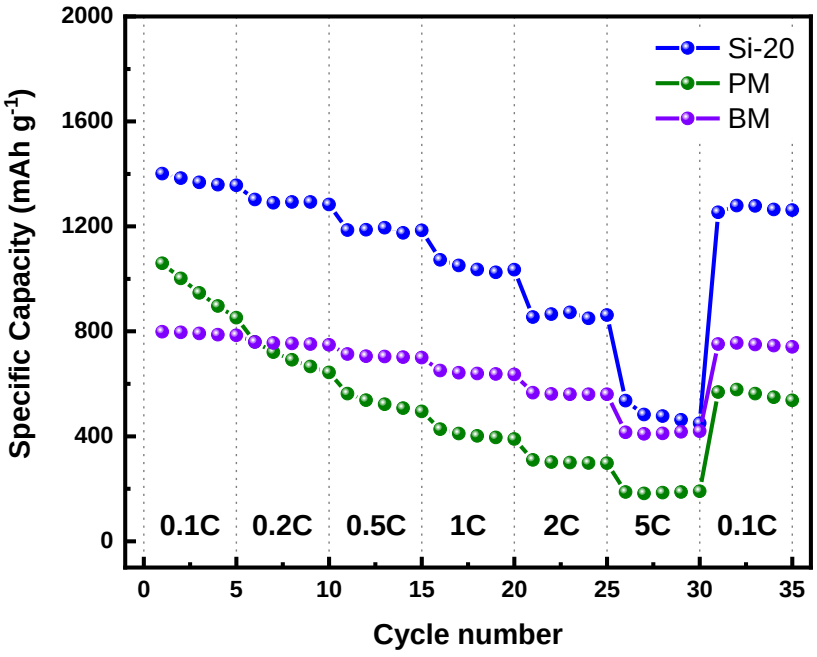

Figure 24. Rate capability of PM, BM, and Si-20

3.5.4. Electrochemical Impedance Spectroscopy analysis

EIS (Electrochemical Impedance Spectroscopy) analysis revealed that the resistance of the BM sample increased compared to the PM and Si-20 samples. This is expected to be due to physical damage during the ball mill process. The PM sample also showed an increase in resistance after the formation of the Solid Electrolyte Interphase (SEI) layer, although not to the extent of the BM sample. In contrast, for the Si-20 sample with adjusted silicon content, a very low resistance value of 5.96 ohms was measured, which is significantly lower when compared to other samples.

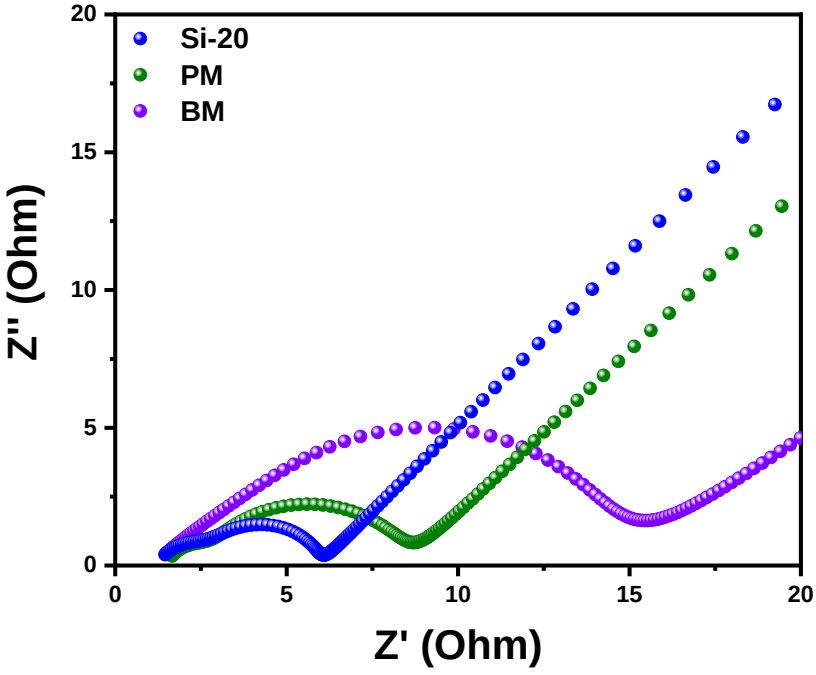

Figure 25. Nyquist plots of PM, BM, and Si-20

Sample	Resistance, R (Ω)			
	R_S	R_{SEI}	R_{ct}	R_{total}
Si-20	1.26	1.57	3.13	5.96
PM	1.54	1.14	5.76	8.44
BM	1.12	6.52	7.34	14.98

Table 1. EIS results of PM, BM, and Si-20

3.6. After Cycle Microscopic Analysis

3.6.1. FE-SEM Analysis

To assess the stability of the anode material, the electrode surfaces before and after 50 cycles were compared using SEM. In the case of the pure silicon electrode, significant damage with large cracks was observed when comparing before and after charge/discharge tests. For the BM sample, although not as extensive as the pure silicon case, some cracks were evident despite appearing stable in the initial cycle test results. However, in the case of the Si-20 sample in this study, stability without visible cracking was confirmed even after 50 cycles, distinguishing it from other samples. Additionally, after 100 cycles, ion milling was employed to measure the cross-sectional volume expansion. The material thickness of the electrode before the cycle test was 24 micrometers, whereas after the cycle test, it increased to 32 micrometers. This result, compared with the theoretical volume expansion rate of 300%[], signifies the successful inhibition of volume expansion, forming a stable electrode with a spherical silicon-graphene oxide structure.

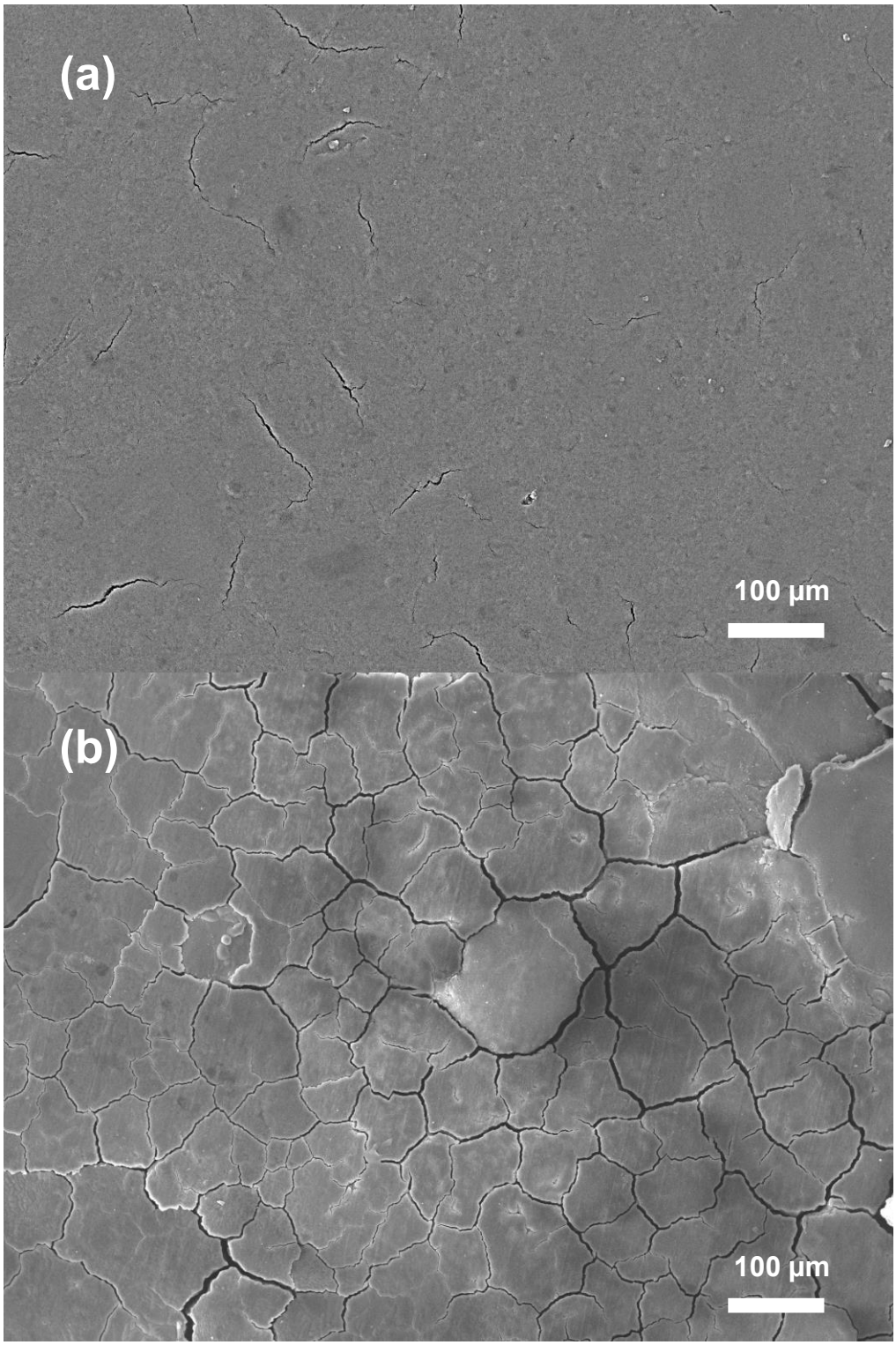

Figure 26. FE-SEM images of Pure Si electrode (a) before and (b) after 50 cycle test

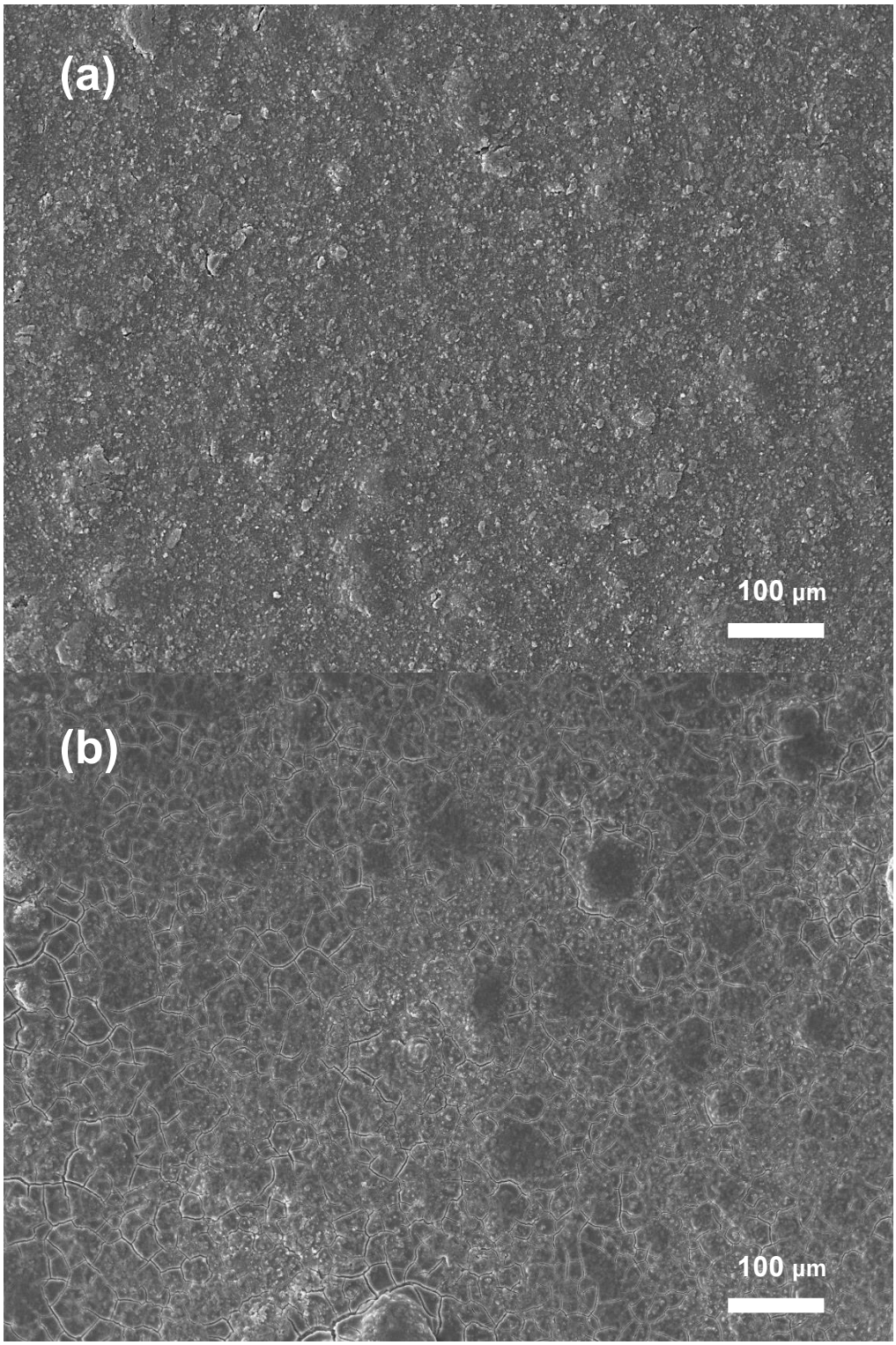

Figure 27. FE-SEM images of BM electrode (a) before and (b) after 50 cycle test

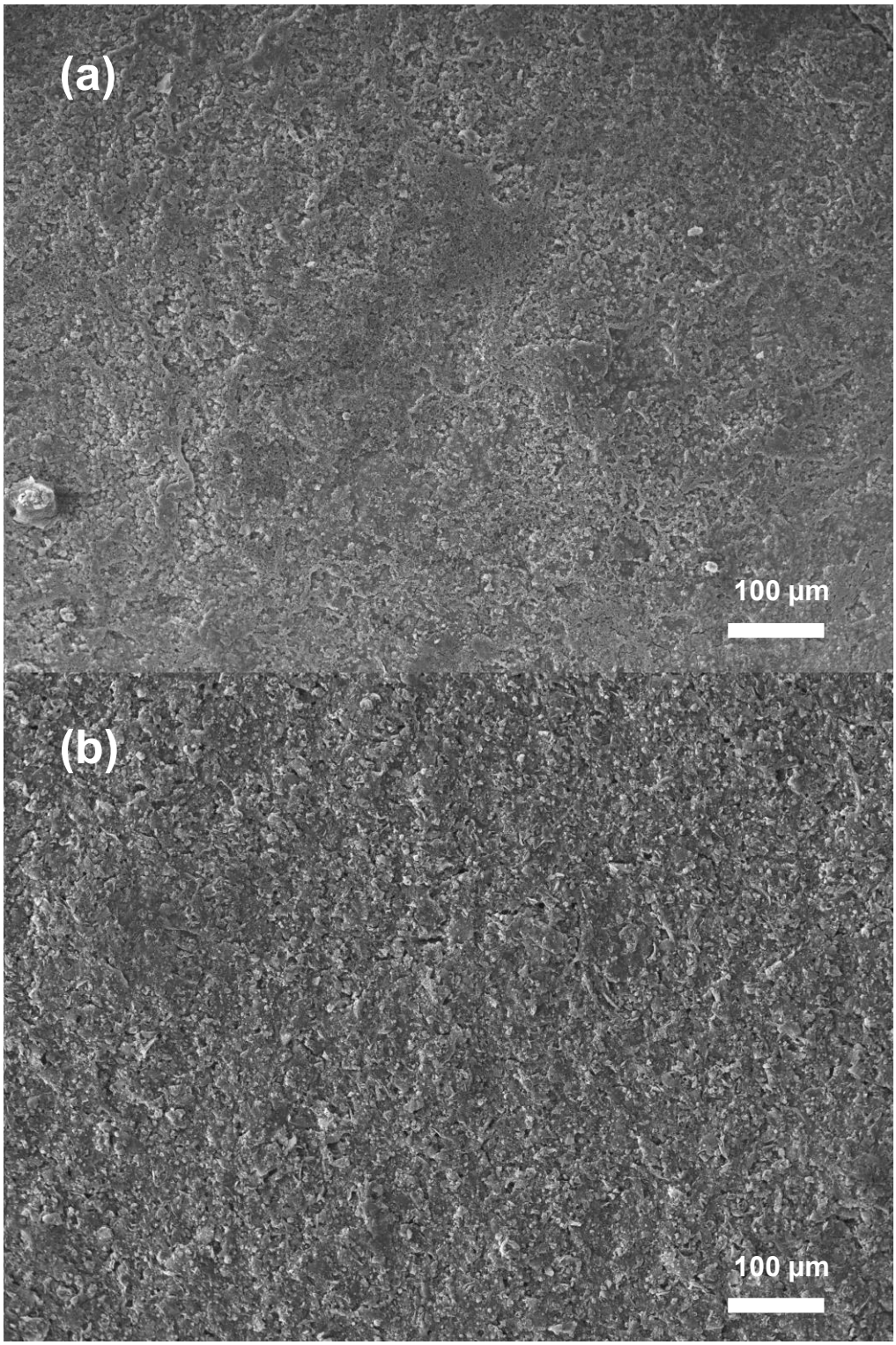

Figure 28. FE-SEM images of Si-20 electrode (a) before and (b) after 50 cycle test

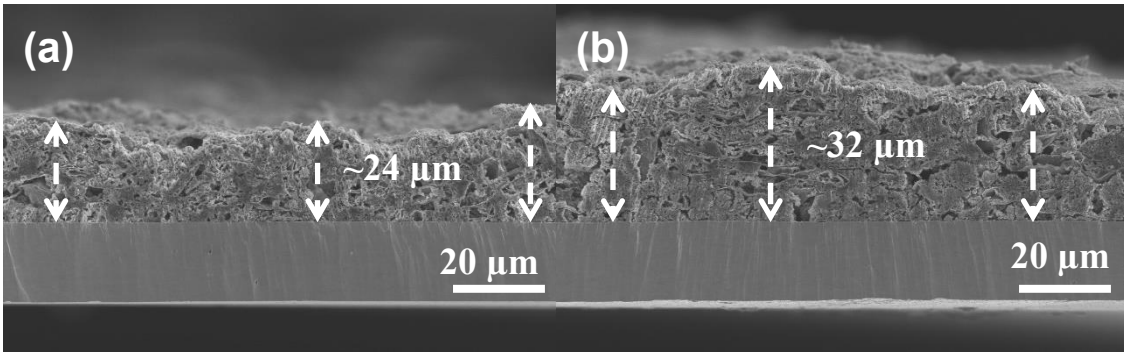

Figure 29. FE-SEM cross-section images of Si-20 electrode (a) before and (b) after 100 cycle test

3.6.2. FE-TEM/EDS Analysis

After 100 cycles, TEM analysis of the sample revealed that, despite the breakage of silicon within the graphene layers, the externally coated carbon and graphene layers maintained the particle structure. Through this observation, it can be confirmed that the spherical structure is maintained stably even after charge and discharge cycles.

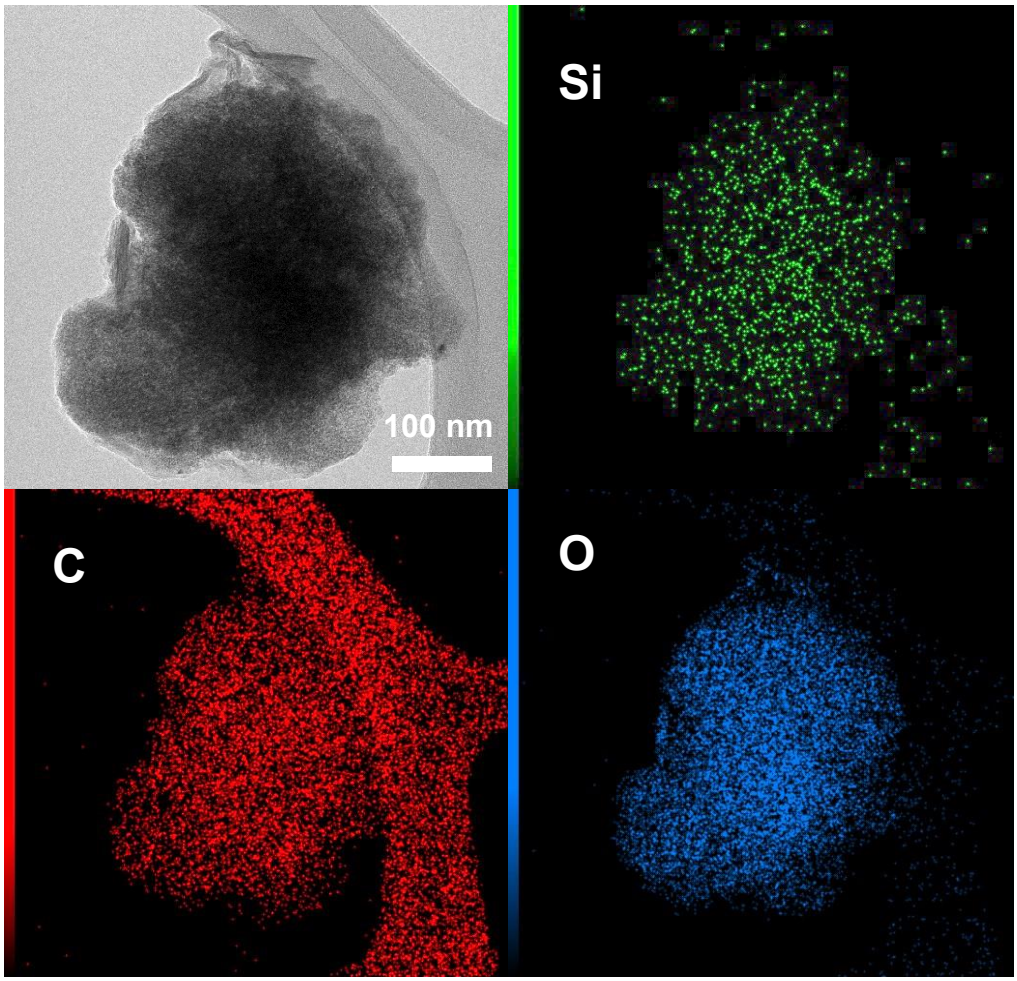

Figure 30. FE-TEM and EDS mapping images of Si-20 after 100 cycle test with elements as Si, C, and O

CHAPTER 4. Conclusion

Successfully synthesized Si/C/rGO particle structure composites using ball milling and spray drying methods, it was confirmed through SEM, TEM, and various analysis techniques that a Si/C/rGO composite with a structure where carbon and rGO encapsulate silicon in a spherical form was formed. In cycle test results, the Si-20 sample maintained its capacity without a decrease, and approximately 65% capacity retention was observed after 250 cycles. When comparing physically mixed, ball-milled, and spray-dried samples, it was noted that using only the ball milling method provided physical stability by embedding silicon particles in graphene oxide sheets, but an increase in internal resistance was observed. However, the issue of increased resistance due to ball milling was successfully addressed by combining it with spray drying, maintaining stability. This is attributed to the deformed spherical structure by the spray dryer method. The electrode produced using this method showed no cracks on the electrode after cycle testing, as confirmed by SEM, and exhibited a volume expansion rate of 140% compared to the theoretical expansion rate of 300%. Additionally, TEM measurements verified the preservation of the electrode structure even after cycle test.

REFERENCES

[1] Lu, L., Han, X., Li, J., Hua, J., & Ouyang, M. (2013). A review on the key issues for lithium-ion battery management in electric vehicles. Journal of power sources, 226, 272-288.

[2] Fasakin, O., Oyedotun, K. O., Kebede, M., Rohwer, M., Le Roux, L., Mathe, M., ... & Manyala, N. (2020). Preparation and physico-chemical investigation of anatase TiO2 nanotubes for a stable anode of lithium-ion battery. Energy Reports, 6, 92-101.

[3] Kasavajjula, U., Wang, C., & Appleby, A. J. (2007). Nano-and bulk-silicon-based insertion anodes for lithium-ion secondary cells. *Journal of power sources*, *163*(2), 1003-1039.

[4] Liu, L., Li, M., Chu, L., Jiang, B., & Lin, R. (2019). Facile fabrication of flexible Si-based nanocomposite films as high-rate anodes by layer-by-layer self-assembly. *Applied Surface Science*, *476*, 501-512.

[5] Muralidharan, N., Self, E. C., Nanda, J., & Belharouak, I. (2022). Next-generation cobalt-free cathodes–a prospective solution to the battery industry's cobalt problem. *Transition Metal Oxides for Electrochemical Energy Storage*, 33-53.

[6] Jung, C.-H., Kim, K.-H., & Hong, S.-H. (2019). Stable silicon anode for lithium-ion batteries through covalent bond formation with a binder via esterification. *ACS applied materials & interfaces*, *11*(30), 26753-26763.

[7] Boukamp, B., Lesh, G., & Huggins, R. (1981). All-solid lithium electrodes with mixed-conductor matrix. *Journal of the Electrochemical Society*, *128*(4), 725.

[8] Uchida, S., Mihashi, M., Yamagata, M., & Ishikawa, M. (2015). Electrochemical properties of non-nano-silicon negative electrodes prepared with a polyimide binder. *Journal of power sources*, *273*, 118-122.

[9] Peng, J., Li, W., Wu, Z., Li, H., Zeng, P., Chen, G., Chang, B., Zhang, X., & Wang, X. (2022). Si/C composite embedded nano-Si in 3D porous carbon matrix and enwound by conductive CNTs as anode of lithium-ion batteries. *Sustainable Materials and Technologies*, *32*, e00410.

[10] An, Y., Tian, Y., Zhang, Y., Wei, C., Tan, L., Zhang, C., Cui, N., Xiong, S., Feng, J., & Qian, Y. (2020). Two-Dimensional Silicon/Carbon from Commercial Alloy and CO2 for Lithium Storage and Flexible Ti3C2T x MXene-Based Lithium–Metal Batteries. *ACS nano*, *14*(12), 17574-17588.

[11] Franco Gonzalez, A., Yang, N.-H., & Liu, R.-S. (2017). Silicon anode design for lithium-ion batteries: progress and perspectives. *The Journal of Physical Chemistry C*, *121*(50), 27775-27787.

[12] Luo, J., Zhao, X., Wu, J., Jang, H. D., Kung, H. H., & Huang, J. (2012). Crumpled graphene-encapsulated Si nanoparticles for lithium ion battery anodes. *The journal of physical chemistry letters*, *3*(13), 1824-1829.

[13] Szczech, J. R., & Jin, S. (2011). Nanostructured silicon for high capacity lithium battery anodes. *Energy & Environmental Science*, *4*(1), 56-72.

[14] Li, Y., Yan, K., Lee, H.-W., Lu, Z., Liu, N., & Cui, Y. (2016). Growth of conformal graphene cages on micrometre-sized silicon particles as stable battery anodes. *Nature Energy*, *1*(2), 1-9.

[15] Wong, D. P., Tseng, H.-P., Chen, Y.-T., Hwang, B.-J., Chen, L.-C., & Chen, K.-H. (2013). A stable silicon/graphene composite using solvent exchange method as anode material for lithium ion batteries. *Carbon*, *63*, 397-403.

[16] Basset, D., Matteazzi, P., & Miani, F. (1993). Designing a high energy ball-mill for synthesis of nanophase materials in large quantities. *Materials Science and Engineering: A*, *168*(2), 149-152.

[17] Binesh, N., Babaloo, H., & Farhadian, N. (2023). Microencapsulation: Spray drying. In *Principles of Biomaterials Encapsulation: Volume One* (pp. 271-296). Elsevier.

[18] Ma, C., Wang, Z., Zhao, Y., Li, Y., & Shi, J. (2020). A novel raspberry-like yolk-shell structured Si/C micro/nano-spheres as high-performance anode materials for lithium-ion batteries. *Journal of alloys and compounds*, *844*, 156201.

[19] Shi, L., Pang, C., Chen, S., Wang, M., Wang, K., Tan, Z., Gao, P., Ren, J., Huang, Y., & Peng, H. (2017). Vertical graphene growth on SiO microparticles for stable lithium ion battery anodes. *Nano Letters*, *17*(6), 3681-3687.

[20] Wang, D., Gao, M., Pan, H., Liu, Y., Wang, J., Li, S., & Ge, H. (2014). Enhanced cycle stability of micro-sized Si/C anode material with low carbon content fabricated via spray drying and in situ carbonization. *Journal of alloys and compounds*, *604*, 130-136.

[21] Liu, J., Zhang, Q., Wu, Z. Y., Li, J. T., Huang, L., & Sun, S. G. (2015). Nano-/Microstructured Si/C Composite with High Tap Density as an Anode Material for Lithium-Ion Batteries. *ChemElectroChem*, *2*(4), 611-616.

[22] Lee, J.-I., Choi, N.-S., & Park, S. (2012). Highly stable Si-based multicomponent anodes for practical use in lithium-ion batteries. *Energy & Environmental Science*, *5*(7), 7878-7882.

[23] Wang, W., & Kumta, P. N. (2010). Nanostructured hybrid silicon/carbon nanotube heterostructures: reversible high-capacity lithium-ion anodes. *ACS nano*, *4*(4), 2233-2241.

[24] Bang, B. M., Kim, H., Song, H.-K., Cho, J., & Park, S. (2011). Scalable approach to multi-

dimensional bulk Si anodes via metal-assisted chemical etching. *Energy & Environmental Science*, *4*(12), 5013-5019.